We are IntechOpen, the world's leading publisher of Open Access books Built by scientists, for scientists

6,900
Open access books available

185,000
International authors and editors

200M
Downloads

Our authors are among the

154
Countries delivered to

TOP 1%
most cited scientists

12.2%
Contributors from top 500 universities



WEB OF SCIENCE™

Selection of our books indexed in the Book Citation Index in Web of Science™ Core Collection (BKCI)

Interested in publishing with us?
Contact book.department@intechopen.com

Numbers displayed above are based on latest data collected.
For more information visit www.intechopen.com



Chapter 10

Recent Trends in Plasmonic Nanowire Solar Cells

Mohamed Hussein,
Mohamed Farhat Othman Hameed and
Salah S. A. Obayya

Additional information is available at the end of the chapter

http://dx.doi.org/10.5772/67617

Abstract

Light trapping is crucial for low-cost and highly efficient nanowire (NW) solar cells (SCs). In order to increase the light absorption through the NWSCs, plasmonic materials can be incorporated inside or above the NW design. In this regard, two novel designs of plasmonic NWSCs are reported and analyzed using 3D finite difference time domain method. The geometrical parameters of the reported designs are studied to improve their electrical and optical efficiencies. The ultimate and power conversion efficiencies (PCE) are used to quantify the conversion efficiency of the light into electricity. The first design relies on funnel shaped SiNWs with plasmonic core while the cylindrical NWs of the second design are decorated by Ag diamond shaped. The calculated ultimate efficiency and PCE of the plasmonic funnel design are equal to 44% and 18.9%, respectively with an enhancement of 43.3 % over its cylindrical NWs counterpart. This enhancement can be explained by the coupling between the three optical modes, supported by the upper cylinder, lower cone and plasmonic material. Moreover, the cylindrical SiNWs decorated by Ag diamond offer an ultimate efficiency and short-circuit current density of 25.7%, and 21.03 mA/cm^2, respectively with an improvement of 63% over the conventional cylindrical SiNWs.

Keywords: light trapping, plasmonic solar cells, nanowires, finite-difference time-domain

1. Introduction

It has become obvious that global stability, economic prosperity, and quality of life are linked intimately with sufficient supplies of clean energy. Searching for energy resources to meet the world's growing demand is a major challenge for the next half century. Traditional energy sources are currently depleted at the rate of approximately 4.1 × 10^{20} J/yr, which is equivalent

INTECH
open science | open minds

© 2017 The Author(s). Licensee InTech. This chapter is distributed under the terms of the Creative Commons Attribution License (http://creativecommons.org/licenses/by/3.0), which permits unrestricted use, distribution, and reproduction in any medium, provided the original work is properly cited. CC BY

to continuous power consumption of 13 trillion watt [1]. An increase in the global population to 9 billion people, along with the rapid worldwide technology development and economic growth, leads to an inevitable increase of more than double the demand for energy (to 30 TW) by 2050 and above the triple demand (to 40 TW) by the end of this century [2]. Because of the dramatic hydrocarbon-based power consumption, the harmful effects (such as global warming, acid precipitation, air pollution, ozone depletion, and forest destruction) are increasingly in catastrophic forms. In the pursuit of limiting these drawbacks, suitable actions aimed at reducing the dependence on the fossil fuels are mandatory. The most urgent challenge is in the search for clean and renewable alternative energy resources required for the sustainable development of human civilization. The Sun is the primary source for clean and abundant energy, with nearly 120,000 TW of incident radiations on the earth's surface which has the potential for covering the human needs [3, 4]. This contains 1.5×10^{18} KWh of energy; which is larger than that of the traditional reserves of oil, coal, and gas which form 1.75×10^{15}, 1.4×10^{15}, and 5.5×10^{15} KWh, respectively [5, 6]. Hence, solar radiation annually provides over 100 times the energy supplied by the entire known fossil fuel sources. Harvesting solar power has become the modern trend in worldwide research projects reported in the scientific community [5, 6]. The photovoltaics (PVs) or solar cell (SC) devices are considered a promising technology that converts the sunlight directly into electricity on a very large scale without causing pollution [7]. The PVs are considered attractive and a promising candidate that would significantly contribute in the future global renewable energy sources. The main challenge in the PV devices is the cost reduction per watt with respect to the fossil fuel technologies. The cost/watt ratio of the photovoltaic devices is at least 1.5 times higher than the electricity generated from the fossil fuels [8]. The main factor influencing the cost/watt ratio is the size of the active material, mostly crystalline silicon (c-Si), and the manufacturing process. The 30–40% of cost/watt in the c-Si SCs is mainly due to the silicon substrate.

Until now, over 90% of the photovoltaic market is currently dominated by the c-Si solar cells. A maximum power conversion efficiency of 25.6% has been achieved for the c-Si solar cell which is approaching the Shockley-Queisser theoretical limit of 29.4%. Therefore, further improvement in the Si solar cell efficiency is required to compete with the fossil fuels and other alternative sources of energy [9]. Different efficient and reliable avenues have been used to enhance the solar cell efficiency and reduce the cost/watt ratio [9]. In the attempt to do so, different materials have been used, such as crystalline silicon (c-Si) [10], amorphous silicon (a-Si) [11], gallium arsenide (GaAs) [12], copper indium gallium selenide (CIGS) cadmium telluride (CdTe) [9, 13], GaSb/GaAs quantum rings [14], organic material [15], and tandem solar cells by combining several materials [16]. The c-Si material is commercially used because it is cheap and abundant compared to other materials. However, the absorption of the c-Si is poor, and a very large thickness is needed to absorb the solar energy. The bandgap of silicon (1.12 eV) is not at the perfect bandgap for solar spectrum, which severely limits the efficiency of the solar cell. Alternatively, a-Si has a better absorption, and it is usually used for thin-film solar cell materials; however, its efficiency is not higher than the c-Si solar cells. The GaAs has high conversion efficiency up to 30% because its bandgap is close to the optimized bandgap for single absorbed material on the expenses of the high total cost. Also, the cadmium telluride (CdTe) has good conversion efficiency, and the cost can be minimized due to the rapid

technology development based on this material. However, the Cd is a highly polluted material, and it has several drawbacks. Recently, different materials can be used to absorb various spectra of solar energy with high efficiency [17, 18]. However, such multi-junction designs need complicated fabrication techniques and expensive manufacturing processes. Thus, the multi-junction solar cells are difficult to be commercialized in the near future.

Currently, the thicknesses of the crystalline silicon wafers used in solar cell market is about 180–300 μm which affects the total cell price due to the silicon materials and processing. Therefore, thin film solar cells attract a great attention, with film thickness in the range of 1–2 μm, as it can be deposited on cheap substrates such as glass, plastic, or stainless steel. However, thin-film solar cell suffers from its weak absorption near the material bandgap especially when using indirect bandgap materials (Si). One of the most alternative important approaches to increase the thin-film solar cell efficiency is the light-trapping techniques to enhance the light absorption into the solar cell active materials. These techniques can increase the light path of the trapped photons in the solar cell materials to generate the electron-hole pair under light illumination. Consequently, the material cost can be minimized by using cheap substrate and solar cell materials with high efficiency. Further, semiconductor nanowires with a few nanometers in diameters can reduce SC material cost with high efficiency. The antireflection layers can be also used to improve the light transmission efficiency [19]. The refractive index of the antireflection layer is chosen between the refractive indices of the active material and surrounding air. The most widely used antireflection materials include SiO_2, SiNx, TiO_2, Al_2O_3, CeO_2, etc. [20]. The antireflection layer can be merged with the textured structures for better light-trapping improvements. The textured silicon surface structures can be etched by various etchants, such as NaOH [21], TMAH [22, 23], and KOH [24]. Different textured structures have been introduced, including the pyramidal textured surfaces [25], inverted pyramidal [26], honeycomb [27], nanowire [28, 29], gratings [30], V-grooved [31], and other types of structures [32–34]. Most of these structures have large size and are not suitable for thin-film SCs with micrometer or sub-micrometer ranges [30]. Recently, the plasmonic SCs attract sharp attention because it can be used for efficient light trapping through the active layer of the SC. Further, it is simple to merge the plasmonic materials into nanowire and thin-film SC designs [35]. Therefore, the plasmonic nanoparticles are considered as pivotal cornerstone in increasing the light trapping in thin-film and nanowire SCs.

Following this introduction, a review of plasmonic light-trapping techniques for solar cell applications will be discussed. In addition, the recent trends in NW SCs are introduced thoroughly. Further, two novel designs of plasmonic NW SCs are presented and analyzed using 3D full-vectorial finite-difference time-domain method (FDTD). In this regard, plasmonic funnel-shaped SiNWs and plasmonic diamond SiNWs are investigated to present the effect of adding plasmonic materials through or above the SiNWs. The performance of the suggested NWSCs has been investigated in terms of the ultimate efficiency and short-circuit current density, open-circuit voltage, power conversion efficiency, and absorbed field profiles. The reported funnel-shaped SiNWs with plasmonic core show an ultimate efficiency of 36.9% which is higher than cylindrical and conical counterparts by 36.7 and 22.2%, respectively. Further, the plasmonic funnel-shaped design has short-circuit current density of 30.2 mA/cm^2 which is greater than 24.5 and 22.12 mA/cm^2 of the conical and cylindrical designs. The

enhancement in the ultimate efficiency and hence short-circuit current density apparently can be attributed to the combination between three types of optical modes that are supported by the upper cylinder, the lower tapered cone, and the plasmonic material. On the other hand, the SiNW decorated by Ag diamond shows an ultimate efficiency of 25.7% which is higher than conventional SiNWs without plasmonic material by 63%. Additionally, the reported design with Ag diamond shows short-circuit current density of 21.03% mA/cm^2 which is greater than the conventional counterpart SiNWs with an improvement of 32.6%.

2. Review of plasmonic light trapping for solar cell applications

At the emergence of the eighteenth century, metallic nanoparticles have gained much interest in the research community for their optical properties. Years later, the Raman scattering was enhanced through the utilization of metallic structures [36] which attracted more researchers to the field of plasmonic nanoparticles. Since then, plasmonic resonance, with its fundamental properties, has been introduced to various applications such as integrated optics, biosensing [37, 38], and energy harvesting [39–41]. In metallic nanoparticles, plasmon resonances give rise to a resonance scattering which reduces the reflection over the spectral range. This anti-reflection effect, caused by random and periodic arrays of metallic nanoparticles, has been extensively studied, theoretically and experimentally, for photovoltaic applications [42, 43]. Stuart and Hall have led the research work in the field of light-sensitive devices enhanced by plasmonic resonance where an enhancement factor of 18 has been reported for a silicon-on-insulator photodetector at 800 nm wavelength. This device has a thickness of 165 nm and is covered by silver nanoparticles on its surface [44]. Additionally, Schaadt et al. [45] proposed a highly doped wafer-based solar cells coated by gold nanoparticles on its surface which achieved an enhancement of 80% for the photocurrent at 500 nm wavelength. Gold nanoparticles have been also used in amorphous thin-film silicon SCs, by Derkacs et al. [43], which improved the overall power conversion efficiency (PCE) by 8%. Pillai et al. [46] achieved 19 and 33% increase in the overall photocurrent for wafer-based SCs and 1.25 μm thick silicon-on-insulator design, respectively, using silver nanoparticles on the cells' surface. Ouyang et al. [47] employed self-assembled Ag nanoparticles on the surface of thin-film silicon SCs which enhanced the short-circuit current density by 27%. A relative photocurrent enhancement of 10% was reported by Beck et al. [48] for silicon cell of thickness 22 μm covered by an array of Ag nanoparticles. In recent years, Tan et al. [49] used Ag nanoparticles as a plasmonic back reflector which offered a net short-circuit current density gain of 2 mA/cm^2. Moreover, different types of solar cells have achieved a performance enhancement based on the plasmonic effect of metallic nanoparticles such as organic and dye-sensitized SCs [50, 51]. In a pioneering breakthrough by Ding et al. [52], plasmonic effect was used to enhance the light absorption and hence, the efficiency of dye-sensitized SCs which achieved a PCE of 5.9% [52]. For a dye-sensitized TiO_2 film, reported by Hägglund et al. [53], an enhanced carrier generation was achieved by employing gold nanodisc. Rand et al. [54] also introduced organic SCs based on ultrathin film using tiny silver nanoparticles which enhanced the cell efficiency. Furthermore, an efficiency enhancement of 1.7 in magnitude was reported by Morfa et al.

for organic bulk heterojunction solar cells [55]. Another organic SCs proposed by Chen et al. achieved an improved PCE using Au nanoparticles incorporated into anodic buffer layer [56].

3. State of the art of semiconductor nanowire solar cells

The current crystalline Si cells are widely used in the PV market with efficiency in the proximity of 25% [57]. A major dilemma lies in the high material cost. The use of cheaper materials, such as polycrystalline thin films or organic semiconductors, decreases the material cost. The amount of required absorbing material can be further decreased by increasing the concentration of the light through a small area [58]. A dramatic improvement in the fabrication techniques can further minimize the loss mechanism and hence increase the SC efficiency. The use of semiconductor nanoantennas (NAs) or NWs readily fulfills all these requirements. In this regard, the NW SCs with structures of a few nanometers in diameters have been considered for PV power generation. The semiconductor NWs have advantages in terms of optical absorption enhancement [59]. This is mainly due to the small reflectivity of the NW array (NWA) with large open area on the frontal surface. The light is trapped by multiple total internal reflections through each nanoscale cylindrical NW resonator [60]. In 2007, Hu and Chen [59] introduced the cylindrical SiNWs with an ultimate efficiency of 15.5%. The behavior of the semiconductor NWs strongly depends on their structural geometrical parameters [59]. Consequently, intense theoretical studies of the optical absorption are required to maximize the ultimate efficiency of the NWA-based SCs. The NWAs with optimized parameters apparently offer higher broadband absorption than solid films [61]. As the NW diameter, period, and wavelength are of the same order, strong light scattering and further light trapping occur [61]. The modified design presented by C. Lin and Povinelli [62] have enhanced the ultimate efficiency up to 23.84% through increasing the lattice constant to 600 nm [62]. The ultimate efficiency of 20.44% was obtained using partially aperiodic vertically SiNWs [63]. Li et al. [64] accomplished an ultimate efficiency of 30.5% by tuning silicon nanowire parameters. The NWAs with random orientation, length, diameter, and position have been experimentally investigated in 2008 [65]. It has been shown that reflection or backscattering was detected with slight effects on the absorption. The optical properties of vertically aligned silicon NWAs with three types of structural randomness, i.e., random position, diameters, and lengths, were numerically investigated [66]. The NWAs with random position displayed slight absorption enhancement, while those with random diameter or length exhibited a significant absorption enhancement. Therefore, the structural randomness in vertical nanowire arrays can further enhance the optical absorption compared to ordered nanowire arrays. The substantial reflectance and absorption of slanting silicon NWAs attracted attention due to their established applications in SCs [67]. The slanting NWAs achieve a significant suppression of light reflection and an enhancement of light-harvesting ability than the conventional vertical structure. The slanted NWAs offer an ultimate efficiency of 33.45%, which exceeds the 30.5% of optimum vertical SiNWs [67]. Wanget al. [68] also reported an ultimate efficiency of 29.1% by using elliptical SiNWAs. On top of that, an ultimate efficiency of 39.3% is achieved using SiNWs arranged in a decagonal lattice [28]. Additionally, periodic vertical cone arrays

form a promising family of structures that are currently under examination for PV technology. Wang et al. proved that the light absorption can be considerably enhanced by using nanocones [69, 70]. In addition, Ko et al. [71] demonstrated that an ultimate efficiency of 28.9% can be obtained by decreasing the cone bottom diameter to 20 nm. Further, the SiNWs funnel shape achieved an ultimate efficiency of 41.8% [29].

4. Simulation methodology and numerical results

4.1. Plasmonic funnel SiNWs

The optical simulation of the suggested designs is carried out using 3D finite-difference time-domain (FDTD) method via Lumerical FDTD solution software package [72]. The FDTD method is widely used in solar cell applications due to its ability to make the simulation physically realistic through using the multi-coefficient material model. Moreover, the FDTD has the capacity to simulate broadband frequency ranges in a single simulation run. In this study, the 3D FDTD method is employed for investigating the optical properties of the SiNWs over the main region of the solar spectrum [72]. **Figure 1(a)** shows the utilized computational domain for the proposed plasmonic funnel-shaped SiNW unit cell in x-z plane. However, **Figure 1(b)** illustrates the x-y view of the suggested design. The top and bottom of the unit cell are surrounded by perfectly matched layers (PML) boundary conditions, while the unit cell is surrounded by periodic boundary conditions (BCs) along x and y directions to simulate periodic square SiNW array. The width and length of the unit cell are equal to 500 nm, while the height is taken as 4000 nm. In order to achieve high accuracy, fine meshing of $\Delta x = \Delta y = \Delta z = 5$ nm is used, which is less than

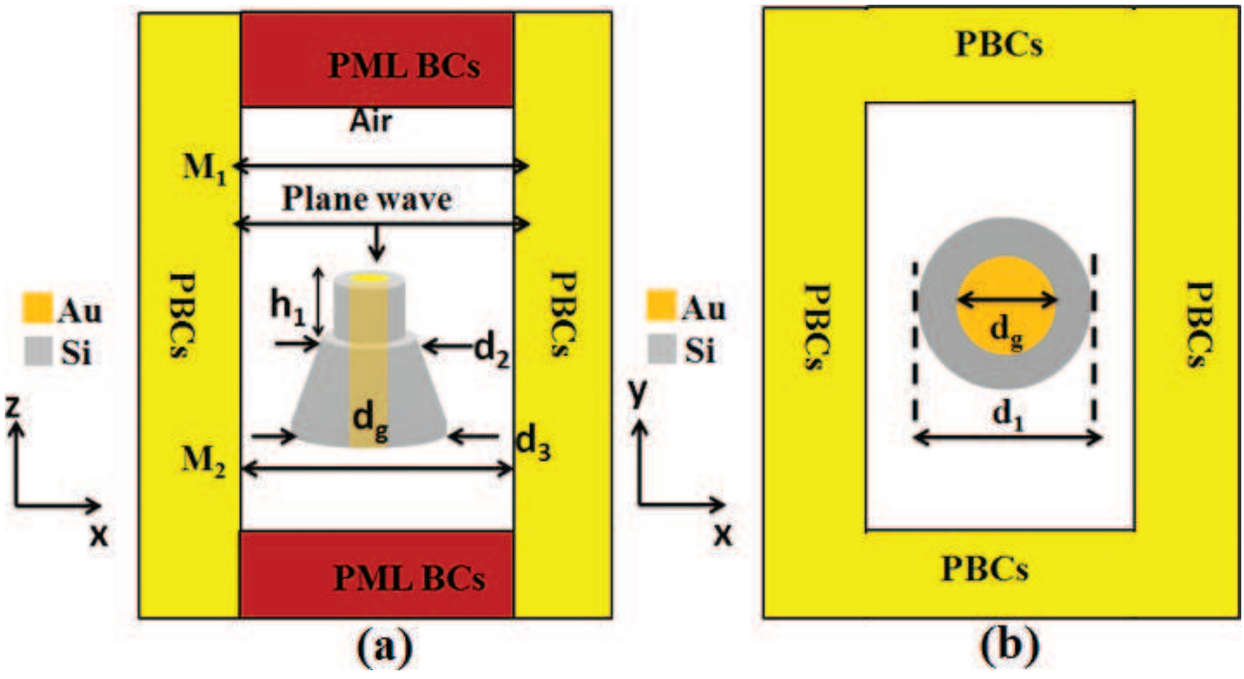


Figure 1. The computational domain of the plasmonic funnel SiNW unit cell in the (a) x-z plane and (b) x-y plane.

1/60 of the shortest wavelength. The proposed plasmonic design is specifically illuminated from the top by a plane wave ranging from 300 to 1100 nm, which covers the main part of the solar spectrum. The incident wave is normal to the x-y plane with the electric field polarized along the x-axis as shown in **Figure 1(a)**. In this study, we only consider lightly doped silicon material. At frequencies above the bandgap, the difference in the optical constants between lightly doped and intrinsic silicon is negligible, which gives us the convenience of using the same optical constants for both p and n regions of the core-shell structure in silicon NW SC [59]. The refractive indices of the SiNWs are taken from experimentally measured optical constants from Ref. [73]. The plasmonic funnel SiNW design shown in **Figure 1** consists of silicon cylinder of height h_1 and a cone of height h_2. The total thickness is equal to h_1+h_2 which is fixed to 2.33 μm that is comparable to the thickness of thin-film solar cell. The Si cylinder has a diameter d_1 with a gold core of diameter d_g, while the cone has upper and lower base diameters of d_2 and d_3, respectively. In this investigation, the NWs are arranged in a square lattice with a periodicity of Λ = 500 nm.

The amount of the total absorbed power by the suggested design can be calculated as a function of the wavelength λ using the total reflection R (λ) and total transmission T (λ) according to the following relation:

$$A(\lambda) = 1\text{-}R(\lambda)\text{-}T(\lambda) \tag{1}$$

Further, the absorbed power by the SiNWs only is calculated as

$$\alpha(\lambda) = \mathbf{A}(\lambda) - \mathbf{Ag}(\lambda) \tag{2}$$

where Ag(λ) is the absorbed power by the plasmonic material. The wavelength-dependent reflection and transmission are calculated by using two frequency domain monitors (M_1) and (M_2), placed above and below the unit cell, respectively, as shown in **Figure 1(a)**. In order to have a convergent absorption, the source and reflection monitors are placed above the SiNWs at a distance 400 and 600 nm, respectively. However, the transmission monitor is placed below the structure by 300 nm. The ultimate efficiency (η) defined as a figure of merit is used to evaluate the absorption capability of the proposed structures for solar cell applications. The ultimate efficiency is calculated from the following equation [4, 8]:

$$\eta = \frac{\int_{300\,\mathrm{nm}}^{\lambda_g} F_s(\lambda)\,\alpha(\lambda)\,\frac{\lambda}{\lambda_g}\,d\lambda}{\int_{300\,\mathrm{nm}}^{4000\,\mathrm{nm}} F_s(\lambda)\,d\lambda} \tag{3}$$

where λ is the wavelength of the incident light, E_g is the bandgap wavelength of the Si, and $F_s(\lambda)$ is the photon flux density in the ASTM AM 1.5 solar spectrum [74]. In this study, λ_g is taken as 1100 nm, corresponding to the energy gap of the silicon material. The short-circuit current density (J_{sc}) is related to the ultimate efficiency by assuming perfect carrier collection efficiency, i.e., each photon absorbed with energy higher than the bandgap produces one electron-hole pair, and all generated carriers are collected to produce current without recombination losses [28, 29]. The short-circuit current density J_{sc} of the proposed design can be expressed as [29]

$$J_{sc} = \eta\frac{q\,\lambda_g}{hc}\int_{300\,\mathrm{nm}}^{4000\,\mathrm{nm}} F_s(\lambda)\,d\lambda = 81.83\eta(mA/c\,m^2) \tag{4}$$

where q is the electron charge, h is Planck's constant, η is ultimate efficiency, and c is the speed of light.

The open-circuit voltage can be related to the maximum short-circuit current density by [75]:

$$V_{oc} = \frac{K_B T_c}{q} \ln\left(1 + \frac{J_{sc}}{J_0}\right), \tag{5}$$

where K_B (ev/K) is the Boltzmann constant, T_c is the ambient temperature of the solar cell temperature that is assumed to be equal to the ambient temperature (i.e., 300 K), and J_0 is the dark saturation current density. The semiempirical expression for the dark saturation current density is given by [75]:

$$J_o = 1.5 \times 10^9 \ln\left(-\frac{E_g}{K_B T_c}\right), \tag{6}$$

The fill factor (FF) is defined as [75]

$$FF = \frac{v_{oc} - \ln(v_{oc} + 0.72)}{v_{oc} + 1}, \tag{7}$$

where $v_{oc} = \frac{V_{oc}}{(KT/q)}$,

To quantify the electrical performance of the proposed design, the power conversion efficiency (PCE) is calculated from the following equation:

$$PCE = \frac{v_{oc} J_{sc} FF}{I_{in}}, \tag{8}$$

where I_{in} is the incident power density at AM 1.5 and is equal to 900.14 w/m^2 [76].

Figure 2(a) depicts the absorption spectra of the cylindrical, conical, and proposed plasmonic funnel NWs versus the wavelength. It should be noted that the absorption of the suggested plasmonic design $\alpha(\lambda)$ shown in this figure is due to the Si only. In this study, d_1 = 300 nm, d_2 = 400 nm, d_g = 120 nm, d_3 = 500 nm, h_1 = 500 nm, and h_2 = 1830 nm. Further, the studied three shapes have the same total height of 2330 nm. It is revealed from this figure that the plasmonic funnel shape shows superior absorption than conical and cylindrical counterparts over the

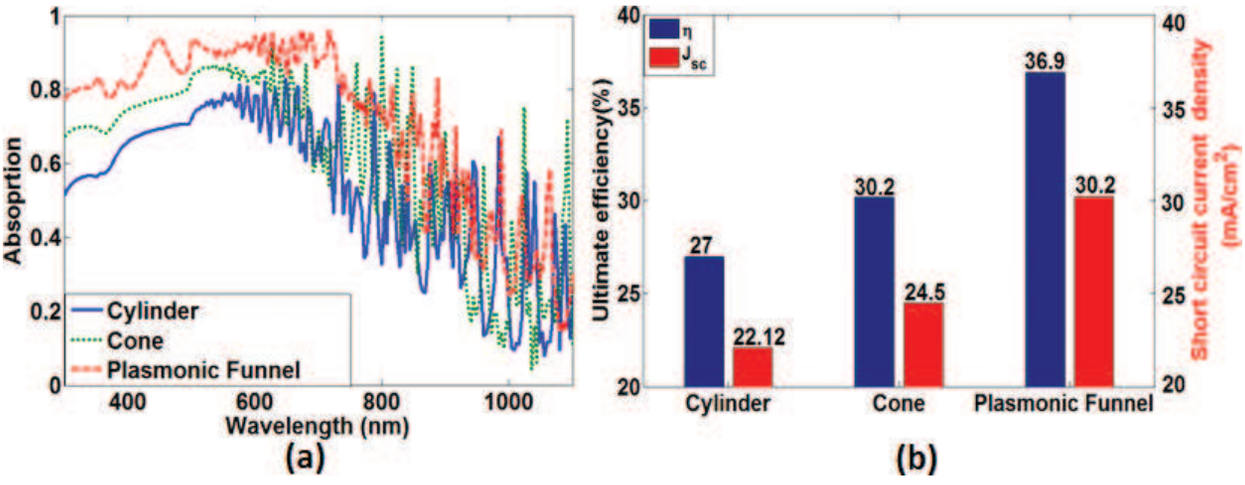


Figure 2. (a) Absorption spectra and (b) ultimate efficiency and short-circuit current density of the cylindrical, conical, and plasmonic funnel NWs.

entire wavelength band. **Figure 2(b)** shows the ultimate efficiency and short-circuit current density of the investigated NWs. The ultimate efficiencies of these structures are equal to 27, 30.2, and 36.9%, respectively. Therefore, it may be noted that the plasmonic funnel-shaped NWs offer an overall enhancement of 36.7 and 22.2% over the cylindrical and conical counterparts. Further, the funnel-shaped design has short-circuit current density of 30.2 mA/cm^2 which is greater than 24.5 and 22.12 mA/cm^2 of the conical and cylindrical designs. The enhancement in the ultimate efficiency and hence short-circuit current density apparently can be attributed to the combination between the modes supported by the upper cylinder and the lower tapered cone along with the plasmonic modes generated by the gold core. Additionally, the proposed design offers continuous reflections between the SiNWs until the incident angle becomes smaller than the critical angle resulting in high light trapping and broadband absorption. Furthermore, the absorption enhancement can be also explained from the waveguide modal dispersion of the NWs [29]. The leaky mode resonance relies on the NW diameter. Therefore, the use of plasmonic funnel-shaped NW with multiple diameters will increase the number of leaky mode resonances. The cylindrical part with small diameter d_1 can absorb short wavelength spectrum. However, the long wavelength spectrum is absorbed by the conical part with upper and lower base diameters d_2 and d_3, respectively. Additionally, the gold core generates plasmonic modes which play an important role for the broadband absorption.

To further confirm the underlying mechanism of the absorption enhancement, the absorbed field profiles inside the cylindrical, conical, and plasmonic funnel shapes have been presented in **Figure 3(a)–(c)**, respectively in x-z plane at λ = 688 nm. It is reveled from these figures that the incident light has more penetration and confinement through the proposed funnel shape with plasmonic core than the conventional conical and cylindrical Si structures. Therefore, the absorption and consequently the ultimate efficiency are enhanced.

In order to ensure that the absorption enhancement of the suggested design is due to the enhanced light trapping in the Si material, the absorption through the plasmonic core and the surrounding Si material are calculated and shown in **Figure 4**. The absorption of the Si NW funnel design [29] without plasmonic material is also plotted in **Figure 4**. It may be noted from this figure that the absorption through the plasmonic metal is small. Further, the plasmonic

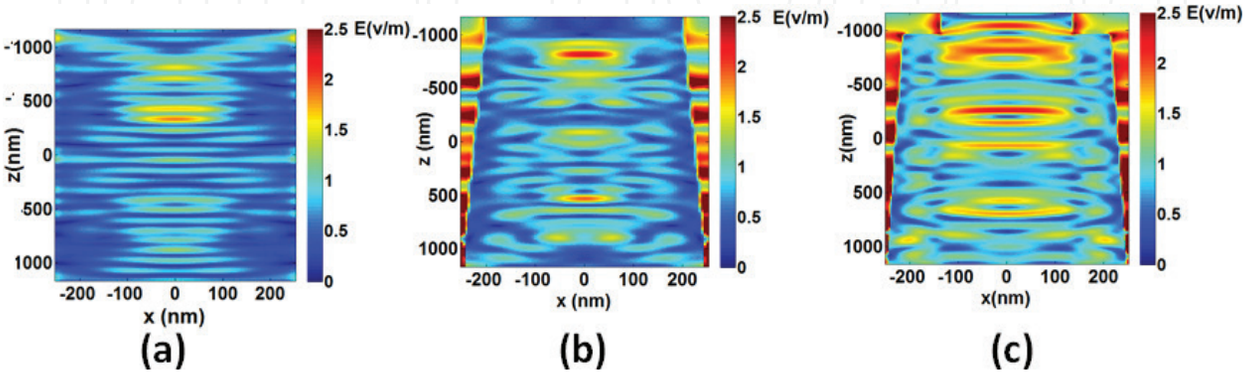


Figure 3. Absorbed field profiles of the (a) cylindrical, (b) conical, and (c) plasmonic funnel SiNWs in x-z plane at λ = 688 nm.

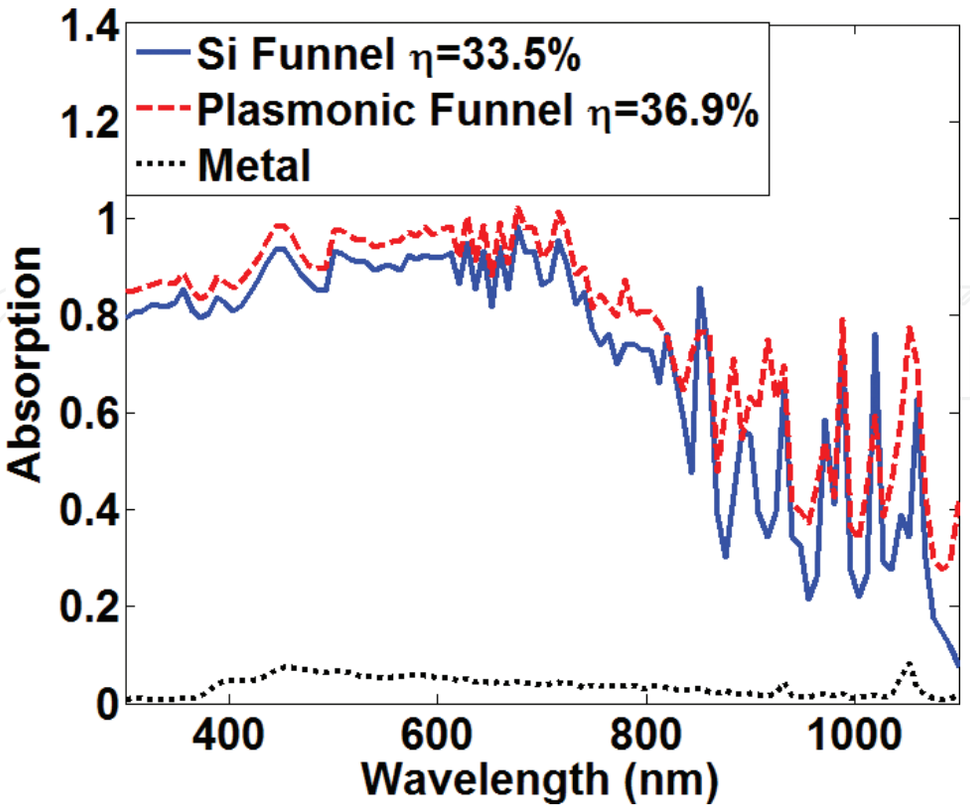


Figure 4. Absorption spectra through the Si funnel [29], metallic layer, and plasmonic funnel NWs.

funnel design has better absorption than that of the Si funnel design [29]. The simulation results also reveal that the plasmonic funnel-shaped NWs achieve an ultimate efficiency of 36.9% which is higher than that of the Si funnel counterpart of ultimate efficiency of 33.5%. The metallic core supports plasmonic modes which increase the light confinement through the silicon NWs. Therefore, the hybrid funnel nanowires improve the light trapping and hence the ultimate efficiency.

To understand the electrical enhancement in the reported design, the ultimate efficiency (η), short-circuit current density (J_{sc}), open-circuit voltage (V_{oc}), fill factor (FF), and power conversion efficiency (PCE) are calculated and shown in **Table 1**. In this table, the calculated values of η, J_{sc}, V_{oc}, FF, and PCE of the cylindrical [66], conical [70], Si funnel [29], and proposed plasmonic funnel SiNWs are listed in detail. It may be noted from this table that the V_{oc} and PCE of the plasmonic funnel shape are higher than that reported in Refs. [29, 66, 70]. Additionally, the PCE of the reported design is higher than that of the cylindrical SiNWs [66] and Si funnel [29] counterparts by 9.95 and 38.2%, respectively. This enhancement is attributed to the better absorption in the plasmonic funnel design which is responsible for enhancing the conversion efficiency. Therefore, the suggested design has a better conversion from optical to electrical power than the previously published design [29, 66, 70].

In order to enhance the absorption capabilities of the proposed funnel-shaped SiNWs with plasmonic core, the effects of the structure geometrical parameters are investigated. **Figure 5(a)** shows the effect of the top cylindrical diameter (d_1) on the ultimate efficiency

Structure	η	J_{sc} (mA/cm²)	V_{oc} (v)	FF	PCE
Cylindrical SiNWs [66]	27%	22.0941	0.6538	0.8380	13.6405
Conical SiNWs [70]	30.2%	24.7127	0.6567	0.8385	15.3247
Funnel SiNWs [29]	33.5%	27.4131	0.6594	0.8390	17.0687
Plasmonic funnel NWs	36.9%	30.1953	0.6619	0.8395	18.8723

Table 1. The ultimate efficiency (η), short-circuit current density (J_{sc}), open-circuit voltage (V_{oc}), fill factor (FF), and power conversion efficiency (PCE) of different structures.

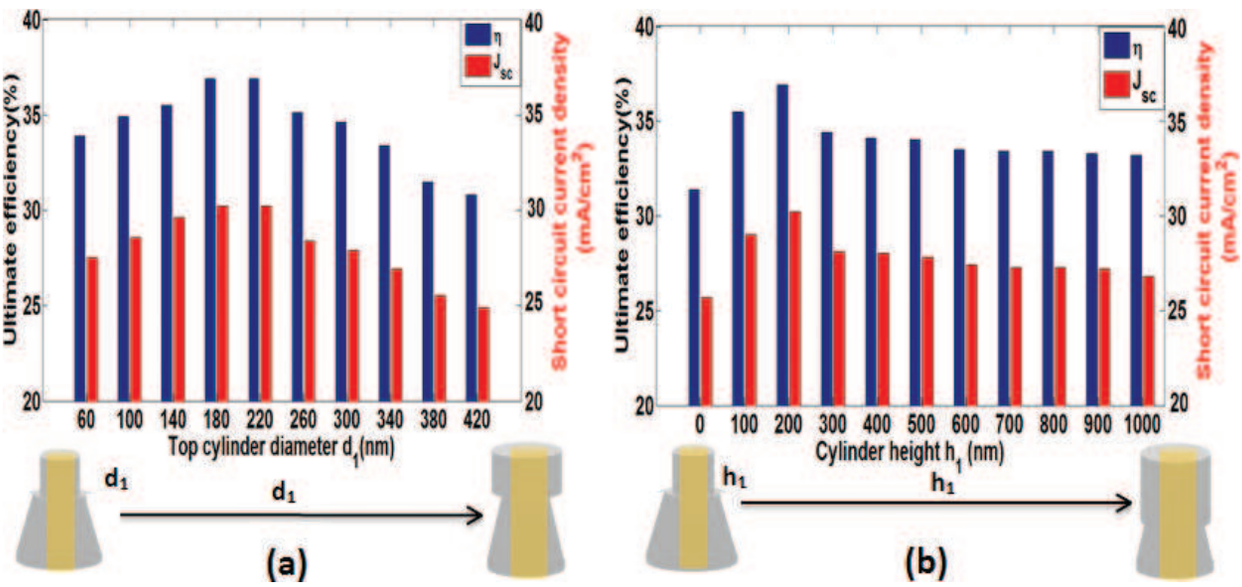


Figure 5. Variation of the short-circuit current density and ultimate efficiency with the (a) cylinder diameter d_1 and (b) cylinder height h_1.

and short-circuit current density for the suggested structure. In this investigation, the other parameters Λ, h_1, d_2, d_3, and h_2 are kept constants at 500, 500, 400, 500, and 1830 nm, respectively. As the diameter (d_1) increases from 60 to 180 nm, the absorption through the SiNWs and hence the ultimate efficiency increase. The ultimate efficiency and short-circuit current density have maximum values of 36.9% and 30.2 mA/cm² at d_1 = 180 nm, respectively. As d_1 is further increased, the reflection will be increased, and hence the absorption and ultimate efficiency are decreased. As a result, the short-circuit current density decreases from 30.2 to 24.9 mA/cm² by increasing d_1 from 180 to 420 nm, respectively. Therefore, the tuned d_1 = 180 nm will be used for the subsequent simulations. Next, the effect of the cylinder height h_1 of the suggested design is also investigated. As h_1 increases from 0 to 200 nm, the ultimate efficiency and short-circuit current density are increased. Therefore, it is concluded that the

funnel shape has a better absorption capability than the conical design at $h_1 = 0$. It may be also seen from **Figure 5(b)** that the cylinder height has a slight effect on the short-circuit current density of the proposed design when $h_1 \geq 300$ nm. This is due to the fixed cylindrical diameter d_1 which faces the incident light. Therefore, the amount of trapped light inside the proposed design is slightly changed with h_1 variation. The maximum ultimate efficiency of 36.9% is obtained at $h_1 = 200$ nm.

Figure 6(a) displays the relation between the short-circuit current density and ultimate efficiency against the cone upper base diameter (d_2) for the suggested design. In this study, the tuned geometrical parameters of the plasmonic design are taken as $d_1 = 180$ nm, $d_3 = 500$, and $h_1 = 200$ nm. As d_2 increases from 160 to 360 nm, the active material increases, and hence higher order optical modes are generated. Therefore, the ultimate efficiency is increased from 33.3 to 36.96%. The tapered shape of the plasmonic design with $d_2 = 360$ nm has maximum ultimate efficiency of 36.9% and J_{sc} of 30.2 mA/cm^2. The effect of the cone base diameter (d_3) is also studied and shown in **Figure 6(b)**. It is revealed from **Figure 6(b)** that as the cone base diameter (d_3) of the plasmonic funnel design increases, the active material will be increased which decreases the transmission through the proposed design. Therefore, the absorption and ultimate efficiency are increased. An optimum ultimate efficiency of 36.9% and J_{sc} of 30.2 mA/cm^2 are obtained at 500 nm cone base diameter.

From the practical point of view, the absorption spectra of the funnel SiNWs with plasmonic core and cylindrical SiNWs decorated on 2 μm Si substrate and Ag back reflector of thickness 200 nm are calculated and shown in **Figure 7**. Compared with the cylindrical SiNWs of ultimate efficiency = 30.6%, the proposed plasmonic design shows an ultimate efficiency of 44% with an enhancements of 43.3% [7]. Additionally, short-circuit current densities of 36 mA/cm^2 and 25.1 mA/cm^2 are achieved by the plasmonic funnel design and cylindrical SiNWs, respectively. This is due to the coupling between the nanowire arrays and underlying substrate which leads to a strong absorption enhancement in the lower energy region as well as good light-trapping improvement in the longer wavelength as displayed in **Figure 7(a)**.

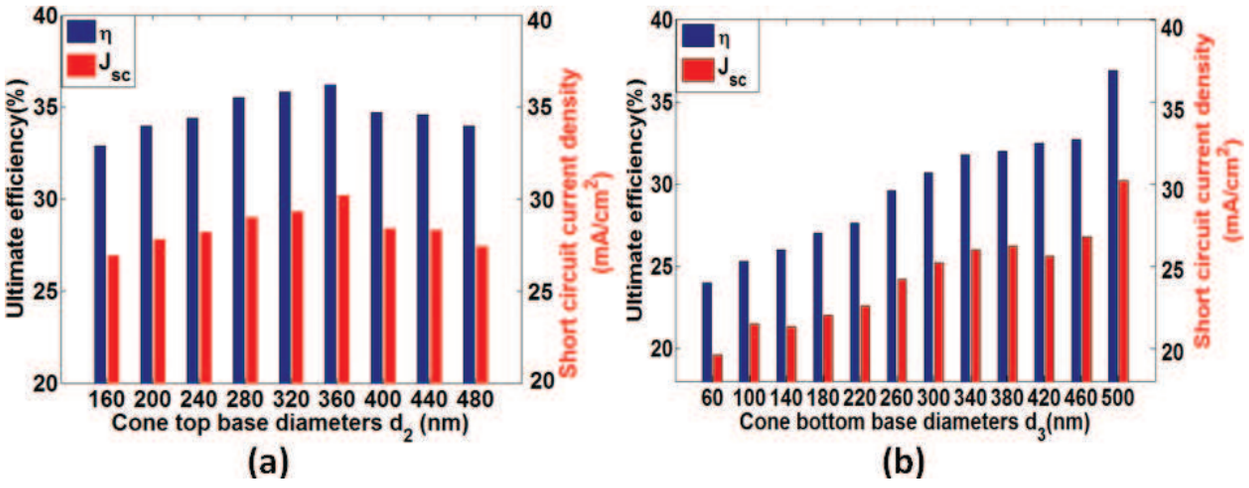


Figure 6. Variation of the short-circuit current density and ultimate efficiency with the cone (a) top diameter d_2 and (b) bottom diameter d_3.

http://dx.doi.org/10.5772/67617

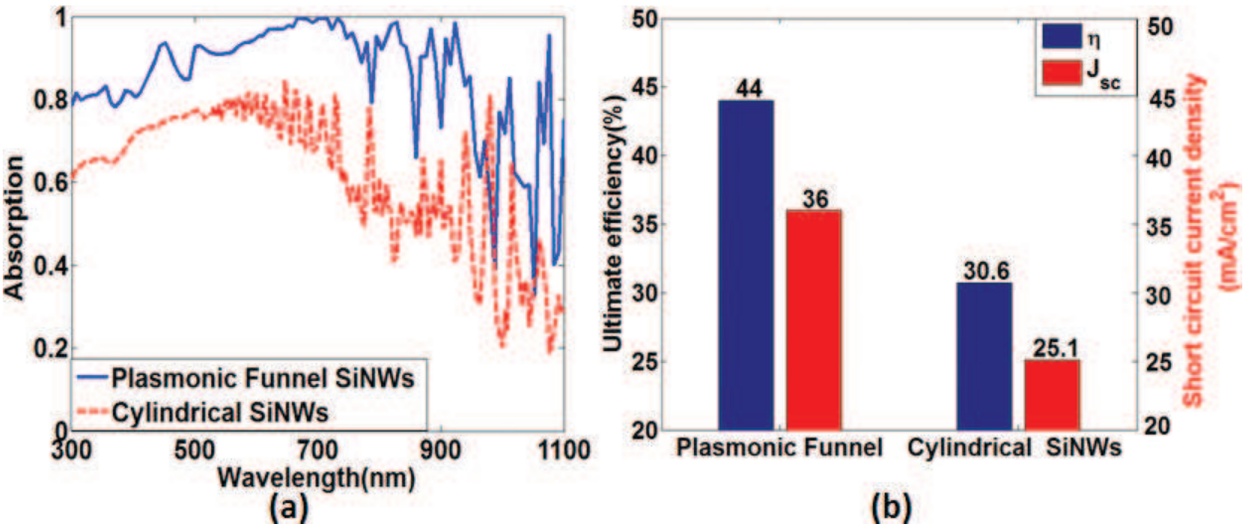


Figure 7. (a) Absorption spectra and (b) ultimate efficiency and short-circuit current density of the proposed plasmonic funnel SiNWs and cylindrical SiNWs with Si substrate and Ag back reflector.

4.2. SiNWs decorated by plasmonic diamond

In order to test the effect of plasmonic material over the NW structure, the cylindrical SiNWs decorated by Ag diamond is studied. **Figure 8(a)** illustrates the computational domain of the proposed plasmonic unit cell in the x-z plane, while **Figure 8(b)** shows the top view of the suggested design. The positive and negative z directions of the unit cell are surrounded by PML boundary conditions, while the unit cell is surrounded by periodic BCs along x

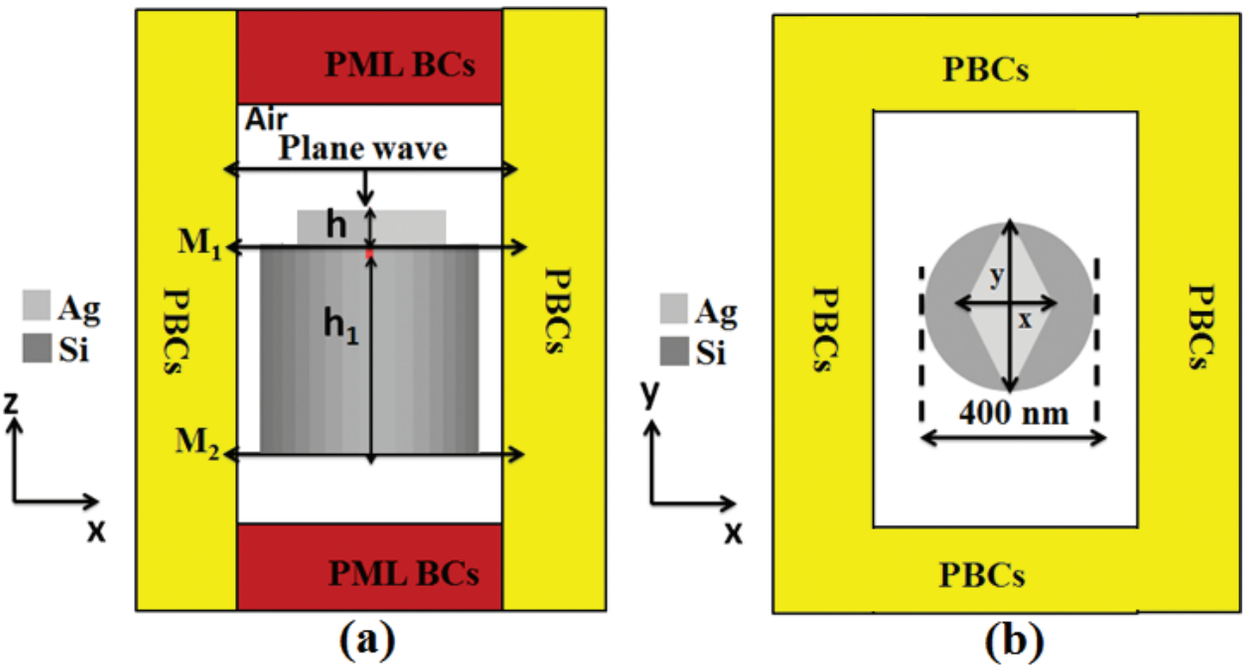


Figure 8. Computational domain of the proposed cylindrical SiNWs decorated by Ag diamond in the (a) x-z plane and (b) x-y plane.

and y directions to simulate periodic square SiNW array. The reported design of the silicon NWs decorated by Ag diamond is specifically illuminated from the top by a plane wave ranging from λ = 300 to 1100 nm, which covers the main part of the solar spectrum. Two frequency-domain field monitors M_1 and M_2 are placed at the top and bottom of the cell, respectively, to calculate the absorption in the SiNW which is defined by $A_{Si} = M_1 - M_2$. In this study, the height and the diameter of the Si nanowire are equal to 500 and 400 nm, respectively. Furthermore, the major and minor axes of the Ag diamond shape are taken as x and y, respectively. In this investigation, x = y = 320 nm, while the diamond thickness h is equal to 80 nm.

Figure 9(a) shows the absorption spectra of the cylindrical SiNWs and cylindrical SiNWs decorated by Ag diamond. It is revealed from this figure that the cylindrical SiNWs with Ag diamond show superior absorption than cylindrical counterpart over the entire wavelength band. Additionally, **Figure 9(b)** shows the ultimate efficiency and short-circuit current density of the studied designs. The ultimate efficiency of the plasmonic design is equal to 21.1% which is greater than the conventional cylindrical design of ultimate efficiency = 16%. Therefore, the cylindrical-shaped design with Ag diamond offers an overall enhancement of 31.9% over the cylindrical SiNWs counterpart. Further, the plasmonic design has a short-circuit current density of 17.3 mA/cm^2 which is greater than that of the conventional cylindrical design of 13.1 mA/cm^2. The enhancement in the ultimate efficiency and hence short-circuit current density can be attributed to the generated plasmonic mode by the upper Ag diamond which is responsible for improving the absorption through the SiNWs.

Table 2 shows the calculated η, J_{sc}, V_{oc}, FF, and PCE of the cylindrical SiNWs and cylindrical SiNWs decorated by Ag diamond. It is found that the electrical parameters are also enhanced due to the existing plasmonic materials above the active layer. Additionally, the V_{oc} is increased from 640 to 647 mV, and the PCE is also improved from 7.9 to 10.6 with 34.1% enhancement over the cylindrical SiNW counterpart.

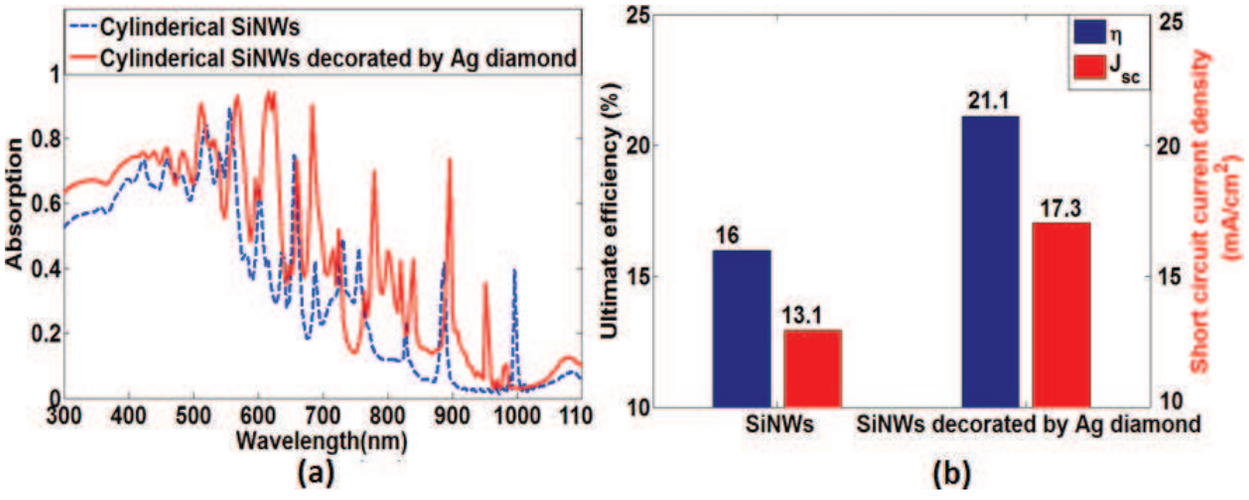


Figure 9. (a) Absorption spectra and (b) ultimate efficiency and short-circuit current density of cylindrical SiNWs and cylindrical SiNWs decorated by Ag diamond.

Structure	η	J_{sc} (mA/cm^2)	V_{oc} (v)	FF	PCE
Cylindrical SiNWs	16%	13.1	0.64	0.835	7.9
Cylindrical SiNWs decorated with Ag diamond	21.1%	17.3	0.647	0.8369	10.6

Table 2. The calculated values of η, J_{sc}, V_{oc}, FF, and PCE for cylindrical SiNWs and cylindrical SiNWs decorated by Ag diamond.

To further explore the underlying mechanism of the absorption enhancement in the proposed design, the field profiles in x-y and x-z planes at λ = 616 nm are shown in **Figure 10**. As shown from **Figure 10(b) and (d)**, the field penetration through the proposed design is greater than that of the conventional SiNWs. This is due to the plasmonic particles that have increased the light confinement around the plasmonic material and, thus, allowed more waveguide modes to couple into the SiNWs which is responsible for the absorption enhancement. Additionally, the figures show high field intensity penetration inside the reported SiNWs which is defined by the field hot spots in the figures.

In order to further enhance the absorption capabilities of the proposed SiNWs decorated by Ag diamond, the effects of the structure geometrical parameters are studied. **Figure 11(a)** shows the impact of the diamond minor axis (x) on the ultimate efficiency and short-circuit current density. In this investigation, the other parameters Λ, h_1, and y are kept constant at 500, 500, 400, and 320 nm, respectively. It is concluded that as the minor axis (x) increases to 280 nm, the absorption and hence the ultimate efficiency and short-circuit current density also increase. A maximum ultimate efficiency and short-circuit current density of 21.4% and 17.5 mA/cm^2, receptively, are obtained at x = 280 nm. If the minor axis is further increased, the ultimate efficiency and short-circuit current density will be decreased. Therefore, the tuned value of 280 nm for the minor axis will be used for the subsequent simulations. Next, the effect of the major axis y of the Ag diamond is also investigated and shown in **Figure 11(b)**. It may be seen from this figure that the ultimate efficiency and short-circuit current density have maximum values of 21.9% and 17.1% at y = 360 nm, respectively. If the major axis y is further increased, the reflection will be increased which decreases the absorption and ultimate efficiency as shown in **Figure 11(b)**.

Next, the effect of the diamond thickness (h) on the ultimate efficiency and short-circuit density is also investigated and shown in **Figure 12(a)**. It is revealed from this figure that the diamond height has a slight effect on the absorption and hence short-circuit current density and ultimate efficiency. A maximum ultimate and short-circuit current density of 22.5% and 18.4 mA/cm^2, respectively, occur at h = 120 nm. **Figure 12(b)** shows the variation of ultimate efficiency and short-circuit density with the periodicity of the NW, while the other parameters are kept constant at h = 120 nm, h_1 = 500 nm, x = 280 nm, and y = 360 nm. As the periodicity decreases, the ultimate efficiency and short-circuit current density increase. The maximum ultimate efficiency of 25.7% is obtained at periodicity of 400 nm which is higher than that of the conventional SiNWs without plasmonic material by 63% at the same periodicity. This enhancement is due to the change of the periodicity which leads to a change in the filling ratio (at fixed diamond size) which in turn influences the generated localized surface plasmon resonance.

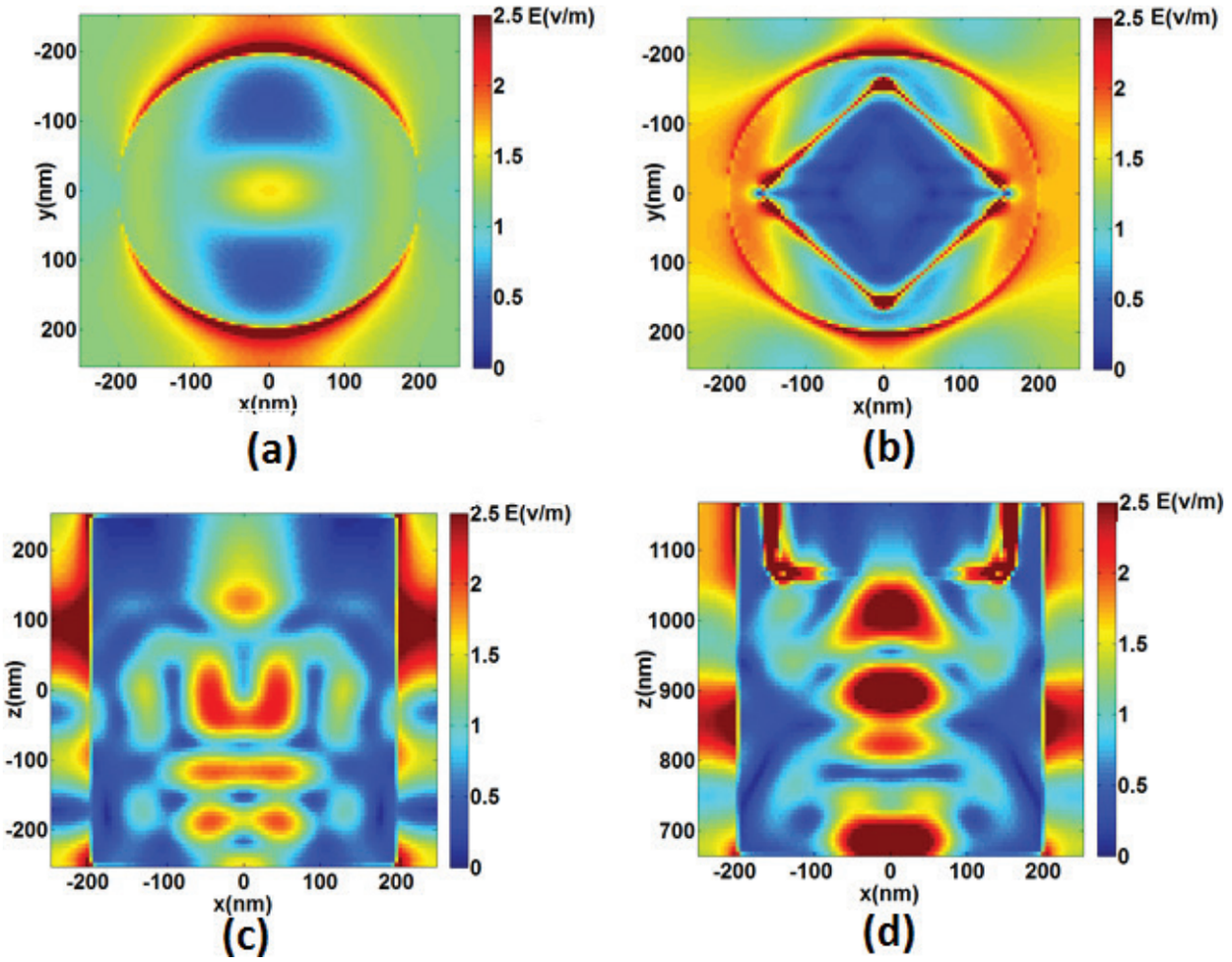


Figure 10. Absorbed field profiles for cylindrical SiNWs without and with Ag diamond particle in the (a, b) x-y plane and in the (c, d) x-z plane at $\lambda = 616$ nm.

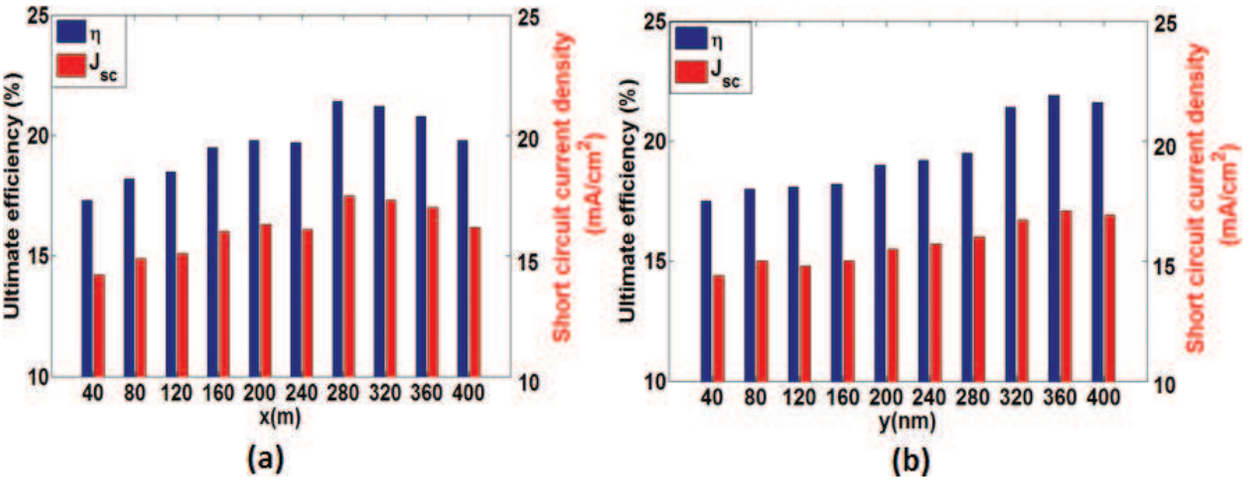


Figure 11. Variation of the short-circuit current density and ultimate efficiency of the conventional SiNWs and SiNWs decorated by Ag diamond with the (a) minor axis x and (b) major axis y.

http://dx.doi.org/10.5772/67617

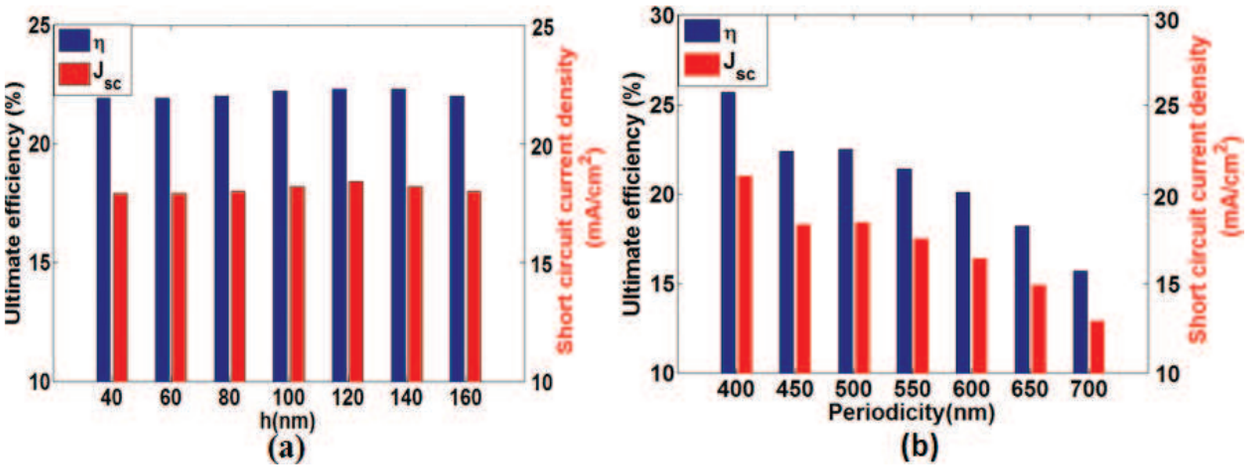


Figure 12. Variation of the short-circuit current density and ultimate efficiency for the conventional SiNWs and SiNWs decorated by Ag diamond with the (a) diamond height and (b) periodicity.

5. Conclusion

In this chapter, the possibility of improving the light trapping through the SiNWs by using plasmonic materials is discussed and studied. In this regard, the effects of using plasmonic materials inside or above the SiNWs are introduced. In these investigations, two novel designs of plasmonic SiNW solar cells are presented and analyzed using the 3D FDTD method. A full study for optical and analytical electrical efficiencies has been carried out. The ultimate efficiency and power conversion efficiency have been calculated to quantify the overall performance of the proposed designs. Further, the designed geometrical parameters are tuned to maximize the optical and electrical efficiencies. The obtained ultimate efficiency and power conversion efficiency of the plasmonic funnel design are equal to 44 and 18.9% with an enhancement of 43.3% over its cylindrical NW counterpart. Additionally, the cylindrical SiNWs decorated by Ag diamond offer an ultimate efficiency and short-circuit current density of 25.7% and 21.03 mA/cm^2, respectively, with an improvement of 63% over the conventional SiNWs. The proposed plasmonic solar cell designs could be very crucial to present low-cost, high-absorption efficiency, and shape-controlled nanopillars for energy-harvesting applications.

Author details

Mohamed Hussein[1,2], Mohamed Farhat Othman Hameed[1,3,] and Salah S. A. Obayya[1,3,*]

*Address all correspondence to: sobayya@zewailcity.edu.eg

1 Centre of Photonics and Smart Materials, Zewail City of Science and Technology, Giza, Egypt

2 Faculty of Science, Ain Shams University, Cairo, Egypt

3 Faculty of Engineering, Mansoura University, Mansoura, Egypt

References

[1] G. Sadashivappa, and N. Sharvari, "Nanoantenna-a review," International Journal of Renewable Energy Technology Research, Vol. 4, pp. 1-9, 2015.

[2] M. A. Khan, P. Sichanugrist, S. Kato, and Y. Ishikawa, "Theoretical investigation about the optical characterization of cone-shaped pin-Si nanowire for top cell application," Energy Science & Engineering, Vol. 4, pp. 383-393, 2016.

[3] L. Mescia, and A. Massaro, "New trends in energy harvesting from earth long-wave infrared emission," Advances in Materials Science and Engineering, Vol. 2014, p. 10, 2014.

[4] F. Manzano-Agugliaro, A. Alcayde, F. G. Montoya, A. Zapata-Sierra, and C. Gil, "Scientific production of renewable energies worldwide: an overview," Renewable and Sustainable Energy Reviews, Vol. 18, pp. 134-143, 2//2013.

[5] A. Arigliano, P. Caricato, A. Grieco, and E. Guerriero, "Producing, storing, using and selling renewable energy: the best mix for the small medium industry," Computers in Industry, Vol. 65, pp. 408-418, 4//2014.

[6] O. D. Miller, "Photonic Design: From Fundamental Solar Cell Physics to Computational Inverse Design," ed, 2012 arXiv:1308.0212 [physics.optics].

[7] W. Wang, J. Zhang, X. Che, and G. Qin, "Large absorption enhancement in ultrathin solar cells patterned by metallic nanocavity arrays," Scientific Reports, Vol. 6, p. 34219, 10/05/online 2016.

[8] W. Raja, A. Bozzola, P. Zilio, E. Miele, S. Panaro, H. Wang ,A. Toma, A. Alabastri, F. Angelis and R. Zaccaria, et al., "Broadband absorption enhancement in plasmonic nanoshells-based ultrathin microcrystalline-Si solar cells," Scientific Reports, Vol. 6, p. 24539, 04/15 11/15/received 03/31/accepted 2016.

[9] S. Foster, and S. John, "Light-trapping design for thin-film silicon-perovskite tandem solar cells," Journal of Applied Physics, Vol. 120, p. 103103, 2016/09/14 2016.

[10] D. M. Powell, M. T. Winkler, H. J. Choi, C. B. Simmons, D. B. Needleman, and T. Buonassisi, "Crystalline silicon photovoltaics: a cost analysis framework for determining technology pathways to reach baseload electricity costs," Energy & Environmental Science, Vol. 5, pp. 5874-5883, 2012.

[11] O. El Daif, E. Drouard, G. Gomard, A. Kaminski, A. Fave, M. Lemiti, et al., "Absorbing one-dimensional planar photonic crystal for amorphous silicon solar cell," Optics Express, Vol. 18, pp. A293–A299, 2010/09/13 2010.

[12] J. Grandidier, D. M. Callahan, J. N. Munday, and H. A. Atwater, "Gallium arsenide solar cell absorption enhancement using whispering gallery modes of dielectric nanospheres," IEEE Journal of Photovoltaics, Vol. 2, pp. 123-128, 2012.

[13] B. Li, J. Liu, G. Xu, R. Lu, L. Feng, and J. Wu, "Development of pulsed laser deposition for CdS/CdTe thin film solar cells," Applied Physics Letters, Vol. 101, p. 153903, 2012/10/08 2012.

[14] P. J. Carrington, M. C. Wagener, J. R. Botha, A. M. Sanchez, and A. Krier, "Enhanced infrared photo-response from GaSb/GaAs quantum ring solar cells," Applied Physics Letters, Vol. 101, p. 231101, 2012/12/03 2012.

[15] J. Cao, Z. Zhan, L. Hou, Y. Long, P. Liu, and W. Mai, "Optical modeling of organic solar cells based on rubrene and C70," Applied Optics, Vol. 51, pp. 5718-5723, 2012/08/10 2012.

[16] D. Shahrjerdi, S. W. Bedell, C. Ebert, C. Bayram, B. Hekmatshoar, K. Fogel, et al., "High-efficiency thin-film InGaP/InGaAs/Ge tandem solar cells enabled by controlled spalling technology," Applied Physics Letters, Vol. 100, p. 053901, 2012/01/30 2012.

[17] A. G. Imenes, and D. R. Mills, "Spectral beam splitting technology for increased conversion efficiency in solar concentrating systems: a review," Solar Energy Materials and Solar Cells, Vol. 84, pp. 19-69, 10//2004.

[18] A. Polman, and H. A. Atwater, "Photonic design principles for ultrahigh-efficiency photovoltaics," Nature Materials, Vol. 11, pp. 174-177, 03//print 2012.

[19] J. A. Dobrowolski, D. Poitras, P. Ma, H. Vakil, and M. Acree, "Toward perfect antireflection coatings: numerical investigation," Applied Optics, Vol. 41, pp. 3075-3083, 2002/06/01 2002.

[20] P. Singh, S. N. Sharma, and N. M. Ravindra, "Applications of porous silicon thin films in solar cells and biosensors," JOM, Vol. 62, pp. 15-24, 2010.

[21] Z. Xi, D. Yang, and D. Que, "Texturization of monocrystalline silicon with tribasic sodium phosphate," Solar Energy Materials and Solar Cells, Vol. 77, pp. 255-263, 5/30/2003.

[22] D. Iencinella, E. Centurioni, R. Rizzoli, and F. Zignani, "An optimized texturing process for silicon solar cell substrates using TMAH," Solar Energy Materials and Solar Cells, Vol. 87, pp. 725-732, 5//2005.

[23] P. Papet, O. Nichiporuk, A. Kaminski, Y. Rozier, J. Kraiem, J. F. Lelievre, et al., "Pyramidal texturing of silicon solar cell with TMAH chemical anisotropic etching," Solar Energy Materials and Solar Cells, Vol. 90, pp. 2319-2328, 9/22/2006.

[24] S. Hayashi, T. Minemoto, H. Takakura, and Y. Hamakawa, "Influence of texture feature size on spherical silicon solar cells," Rare Metals, Vol. 25, pp. 115-120, 2006/10/01 2006.

[25] P. Campbell, and M. A. Green, "Light trapping properties of pyramidally textured surfaces," Journal of Applied Physics, Vol. 62, pp. 243-249, 1987/07/01 1987.

[26] S. C. Baker-Finch, and K. R. McIntosh, "Reflection of normally incident light from silicon solar cells with pyramidal texture," Progress in Photovoltaics: Research and Applications, Vol. 19, pp. 406-416, 2011.

[27] J. Zhao, A. Wang, M. A. Green, and F. Ferrazza, "19.8% efficient "honeycomb" textured multicrystalline and 24.4% monocrystalline silicon solar cells," Applied Physics Letters, Vol. 73, pp. 1991-1993, 1998/10/05 1998.

[28] M. Hussein, M. F. O. Hameed, N. F. F. Areed, and S. S. A. Obayya, "Ultra-high efficient solar cell based on decagonal arrays of silicon nanowires," Optical Engineering, Vol. 53, pp. 117105-117105, 2014.

[29] M. Hussein, M. F. O. Hameed, N. F. F. Areed, A. Yahia, and S. S. A. Obayya, "Funnel-shaped silicon nanowire for highly efficient light trapping," Optics Letters, Vol. 41, pp. 1010-1013, 2016/03/01 2016.

[30] Y.-C. Lee, C.-F. Huang, J.-Y. Chang, and M.-L. Wu, "Enhanced light trapping based on guided mode resonance effect for thin-film silicon solar cells with two filling-factor gratings," Optics Express, Vol. 16, pp. 7969-7975, 2008/05/26 2008.

[31] H. Nakaya, M. Nishida, Y. Takeda, S. Moriuchi, T. Tonegawa, T. Machida, et al., "Polycrystalline silicon solar cells with V-grooved surface," Solar Energy Materials and Solar Cells, Vol. 34, pp. 219-225, 1994/09/01 1994.

[32] X. D. Wang, E. Graugnard, J. S. King, Z. L. Wang, and C. J. Summers, "Large-scale fabrication of ordered nanobowl arrays," Nano Letters, Vol. 4, pp. 2223-2226, 2004/11/01 2004.

[33] J. W. Leem, D. H. Joo, and J. S. Yu, "Biomimetic parabola-shaped AZO subwavelength grating structures for efficient antireflection of Si-based solar cells," Solar Energy Materials and Solar Cells, Vol. 95, pp. 2221-2227, 8//2011.

[34] J. W. Leem, J. S. Yu, Y. M. Song, and Y. T. Lee, "Antireflective characteristics of disordered GaAs subwavelength structures by thermally dewetted Au nanoparticles," Solar Energy Materials and Solar Cells, Vol. 95, pp. 669-676, 2//2011.

[35] H. A. Atwater, and A. Polman, "Plasmonics for improved photovoltaic devices," Nature Materials, Vol. 9, pp. 205-213, 03//print 2010.

[36] S. Nie, and S. R. Emory, "Probing single molecules and single nanoparticles by surface-enhanced Raman scattering," Science, Vol. 275, p. 1102, 1997.

[37] S. A. Maier, M. L. Brongersma, P. G. Kik, S. Meltzer, A. A. G. Requicha, and H. A. Atwater, "Plasmonics—a route to nanoscale optical devices," Advanced Materials, Vol. 13, pp. 1501-1505, 2001.

[38] X. D. Hoa, A. G. Kirk, and M. Tabrizian, "Towards integrated and sensitive surface plasmon resonance biosensors: a review of recent progress," Biosensors and Bioelectronics, Vol. 23, pp. 151-160, 9/30/2007.

[39] M. Hussein, N. F. F. Areed, M. F. O. Hameed, and S. S. A. Obayya, "Design of flower-shaped dipole nano-antenna for energy harvesting," IET Optoelectronics, Vol. 8, pp. 167-173, 2014.

[40] O. Salah, A. Nihal Fayez Fahmy, O. H. Mohamed Farhat, and A. Mohamed Hussein, "Optical nano-antennas for energy harvesting," in Innovative Materials and Systems for Energy Harvesting Applications, M. Luciano, L. Onofrio, and P. Francesco, Eds., Hershey, PA, USA: IGI Global, 2015, pp. 26-62.

[41] Y. M. El-Toukhy, M. Hussein, M. F. O. Hameed, A. M. Heikal, M. M. Abd-Elrazzak, and S. S. A. Obayya, "Optimized tapered dipole nanoantenna as efficient energy harvester," Optics Express, Vol. 24, pp. A1107–A1122, 2016/07/11 2016.

[42] K. Nakayama, K. Tanabe, and H. A. Atwater, "Plasmonic nanoparticle enhanced light absorption in GaAs solar cells," Applied Physics Letters, Vol. 93, p. 121904, 2008.

[43] D. Derkacs, S. H. Lim, P. Matheu, W. Mar, and E. T. Yu, "Improved performance of amorphous silicon solar cells via scattering from surface plasmon polaritons in nearby metallic nanoparticles," Applied Physics Letters, Vol. 89, p. 093103, 2006.

[44] H. R. Stuart, and D. G. Hall, "Island size effects in nanoparticle-enhanced photodetectors," Applied Physics Letters, Vol. 73, pp. 3815-3817, 1998.

[45] D. M. Schaadt, B. Feng, and E. T. Yu, "Enhanced semiconductor optical absorption via surface plasmon excitation in metal nanoparticles," Applied Physics Letters, Vol. 86, p. 063106, 2005.

[46] S. Pillai, K. R. Catchpole, T. Trupke, and M. A. Green, "Surface plasmon enhanced silicon solar cells," Journal of Applied Physics, Vol. 101, p. 093105, 2007.

[47] Z. Ouyang, X. Zhao, S. Varlamov, Y. Tao, J. Wong, and S. Pillai, "Nanoparticle-enhanced light trapping in thin-film silicon solar cells," Progress in Photovoltaics: Research and Applications, Vol. 19, pp. 917-926, 2011.

[48] F. J. Beck, S. Mokkapati, and K. R. Catchpole, "Plasmonic light-trapping for Si solar cells using self-assembled, Ag nanoparticles," Progress in Photovoltaics: Research and Applications, Vol. 18, pp. 500-504, 2010.

[49] H. Tan, R. Santbergen, A. H. Smets, and M. Zeman, "Plasmonic light trapping in thin-film silicon solar cells with improved self-assembled silver nanoparticles," Nano Letters, Vol. 12, pp. 4070-4076, 2012.

[50] L. Lu, Z. Luo, T. Xu, and L. Yu, "Cooperative plasmonic effect of Ag and Au nanoparticles on enhancing performance of polymer solar cells," Nano Letters, Vol. 13, pp. 59-64, 2012.

[51] A. P. Kulkarni, K. M. Noone, K. Munechika, S. R. Guyer, and D. S. Ginger, "Plasmon-enhanced charge carrier generation in organic photovoltaic films using silver nanoprisms," Nano Letters, Vol. 10, pp. 1501-1505, 2010.

[52] I. Ding, J. Zhu, W. Cai, S. J. Moon, N. Cai, P. Wang, et al., "Plasmonic dye-sensitized solar cells," Advanced Energy Materials, Vol. 1, pp. 52-57, 2011.

[53] C. Hägglund, M. Zäch, and B. Kasemo, "Enhanced charge carrier generation in dye sensitized solar cells by nanoparticle plasmons," Applied Physics Letters, Vol. 92, p. 013113, 2008.

[54] B. P. Rand, P. Peumans, and S. R. Forrest, "Long-range absorption enhancement in organic tandem thin-film solar cells containing silver nanoclusters," Journal of Applied Physics, Vol. 96, pp. 7519-7526, 2004.

[55] A. J. Morfa, K. L. Rowlen, T. H. R. III, M. J. Romero, and J. V. D. Lagemaat, "Plasmon-enhanced solar energy conversion in organic bulk heterojunction photovoltaics," Applied Physics Letters, Vol. 92, p. 013504, 2008.

[56] F.-C. Chen, J.-L. Wu, C.-L. Lee, Y. Hong, C.-H. Kuo, and M. H. Huang, "Plasmonic-enhanced polymer photovoltaic devices incorporating solution-processable metal nanoparticles," Applied Physics Letters, Vol. 95, p. 013305, 2009.

[57] R. M. Ferdous, A. W. Reza, and M. F. Siddiqui, "Renewable energy harvesting for wireless sensors using passive RFID tag technology: a review," Renewable and Sustainable Energy Reviews, Vol. 58, pp. 1114-1128, 2016.

[58] J. Nelson, The Physics of Solar Cells. Vol. 1: World Scientific, Imperial College, UK, 2003.

[59] L. Hu, and G. Chen, "Analysis of optical absorption in silicon nanowire arrays for photovoltaic applications," Nano Letters, Vol. 7, pp. 3249-3252, 2007.

[60] L. Cao, P. Fan, A. P. Vasudev, J. S. White, Z. Yu, W. Cai, et al., "Semiconductor nanowire optical antenna solar absorbers," Nano Letters, Vol. 10, pp. 439-445, 2010.

[61] C. Lin, and M. L. Povinelli, "Optical absorption enhancement in silicon nanowire and nanohole arrays for photovoltaic applications," in Proc. SPIE 7772, Next Generation (Nano) Photonic and Cell Technologies for Solar Energy Conversion, 77721G (August 24, 2010); doi:10.1117/12.860254.

[62] C. Lin, and M. L. Povinelli, "Optical absorption enhancement in silicon nanowire arrays with a large lattice constant for photovoltaic applications," Optics Express, Vol. 17, pp. 19371-19381, 2009.

[63] C. Lin, and M. L. Povinelli, "Optimal design of aperiodic, vertical silicon nanowire structures for photovoltaics," Optics Express, Vol. 19, pp. A1148–A1154, 2011.

[64] J. Li, H. Yu, S. M. Wong, X. Li, G. Zhang, P. G.-Q. Lo, et al., "Design guidelines of periodic Si nanowire arrays for solar cell application," Applied Physics Letters, Vol. 95, p. 243113, 2009.

[65] O. L. Muskens, J. G. Rivas, R. E. Algra, E. P. Bakkers, and A. Lagendijk, "Design of light scattering in nanowire materials for photovoltaic applications," Nano Letters, Vol. 8, pp. 2638-2642, 2008.

[66] H. Bao, and X. Ruan, "Optical absorption enhancement in disordered vertical silicon nanowire arrays for photovoltaic applications," Optics Letters, Vol. 35, pp. 3378-3380, 2010.

[67] L. Hong, Rusli, X. Wang, H. Zheng, H. Wang, and H. Yu, "Design guidelines for slanting silicon nanowire arrays for solar cell application," Journal of Applied Physics, Vol. 114, p. 084303, 2013.

[68] R. Ren, Y.-X. Guo, and R.-H. Zhu, "Enhanced absorption in elliptical silicon nanowire arrays for solar energy harvesting," Optical Engineering, Vol. 53, pp. 027102-027102, 2014.

[69] B. Wang, E. Stevens, and P. W. Leu, "Strong broadband absorption in GaAs nanocone and nanowire arrays for solar cells," Optics Express, Vol. 22, pp. A386–A395, 2014.

[70] B. Wang, and P. W. Leu, "Enhanced absorption in silicon nanocone arrays for photovoltaics," Nanotechnology, Vol. 23, p. 194003, 2012.

[71] M.-D. Ko, C.-K. Baek, T. Rim, S. Park, and Y.-H. Jeong, "Optical and electrical characteristics of asymmetric nanowire solar cells," Journal of Applied Physics, Vol. 111, p. 073102, 2012.

[72] F. Lumerical, "Solution, FDTD Solutions 6.5," ed. http://www.lumerical.com/tcad-products/fdtd/

[73] E. D. Palik, Handbook of Optical Constants of Solids Vol. 3: Academic press, Elsevier Inc. 1998.

[74] NREL. Reference Solar Spectral Irradiance: ASTM G-173. Available: http://rredc.nrel.gov/solar/spectra/am1.5/astmg173/astmg173.html. 2016.

[75] Z. Jia, Q. Cheng, J. Song, M. Si, and Z. Luo, "Optical properties of a grating-nanorod assembly structure for solar cells," Optics Communications, Vol. 376, pp. 14-20, 2016.

[76] P. R. Pudasaini, and A. A. Ayon, "Nanostructured thin film silicon solar cells efficiency improvement using gold nanoparticles," Physica Status Solidi (a), Vol. 209, pp. 1475-1480, 2012.

IntechOpen

IntechOpen

IntechOpen